Batteries & Supercaps

Research Article
doi.org/10.1002/batt.202300263

Chemistry Europe
European Chemical Societies Publishing

www.batteries-supercaps.org

A Novel Approach for Development of Stable Quasi-Solid Lithium-O_2 Batteries: Assembly and Performances of Double Layer Gel Polymer Electrolytes

Mustafa Celik,*[a, b] Sara Pakseresht,[a] Ahmed Waleed Majeed Al-Ogaili,[a] Samet Usta,[a, b] Hatem Akbulut,[a, b, c] and Tugrul Cetinkaya[a, b, c]

Gel-polymer electrolytes (GPEs) offer a suitable alternative to flammable organic liquid electrolytes in lithium-oxygen batteries (LOBs) to address safety concerns. However, a major challenge with GPEs is their low ionic conductivity. To enhance the ionic conductivity of GPEs, active inorganic particles have been incorporated. To increase the ionic conductivity of GPE, active inorganic particles have been reinforced in GPE. While this increases the ionic conductivity, it also leads to blockage of the cathode porous structure and reduces the actual surface area of the cathode materials, resulting in poor battery performance. This study proposes a novel double-layer polymer gel electrolyte (d-GPE) that exhibits both high ionic conductivity and stability for quasi solid-state LOBs. The double-layer GPE consists of a bare GPE layer integrated in the cathode, and a composite GPE (c-GPE, containing 5 wt.% lithium aluminum titanium phosphate (LATP)), which is in contact with Li anode and bare-GPE. The produced double-layer gel polymer electrolyte displays high reaction kinetic and better stability due to the excellent electrode/electrolyte interface and rapid oxygen diffusion in the air-cathode. Furthermore, the d-GPE electrolyte is resistant to fire and protects Li from dendrite growth and water molecules attack, indicating tremendous promise for the development of practical LOBs.

Introduction

The widespread use of electronic devices and high energy demand trigger the development of extremely efficient and high energy density batteries. Lithium-oxygen batteries (LOBs) have become a promising battery technology for this requirement. LOB has a high theoretical specific energy of about 11400 Wh kg^{-1}, which is ten times higher than a lithium-ion battery (LIBs).[1,2] Aqueous and non-aqueous LOBs have been intensively investigated as energy systems. However, their practical application is hindered as a power source due to leakage, volatility, and flammability of liquid electrolyte, as well as lithium anode corrosion from reactivity with liquid electrolyte and oxygen flow from the cathode side. Many studies have been indicated that most liquid electrolytes are not stable enough toward the discharge products at the cathode side, therefore leading to the decomposition of electrolytes and formation of by-products, which limit the cycle performances of the battery. Furthermore, the generation and constant growth of lithium dendrites in a liquid electrolyte system have been recognized as a cause of cell malfunction and danger.[3] Hence, utilizing conductive solid electrolytes with high density can be an effective solution to replace liquid electrolytes and enhance cycling performance and safety concerns of LOBs.[4–7] Solid electrolytes, such as polymer and ceramic electrolytes, have been considered viable replacements for LOB liquid electrolytes. Ceramic electrolytes, such as NASICON-type Li-Al-Ge phosphate (LAGP)[8,9] and Li-Al-Ti phosphate (LATP), have good ion conductivity, but their use has been hampered due to their inherent fragility and expensive cost.[10,11] On the other hand, polymer-based electrolytes have been extensively explored as one of the most advantageous solid-state electrolytes due to their high safety, enhanced shape flexibility, good mechanical strength, good adhesion, stable electrochemical voltage window, and low interfacial charge-transfer resistance.[12–15] Many polymers and copolymers have been used as polymer-based electrolytes in lithium batteries consisting of polyethylene oxide (PEO), polymethyl methacrylate (PMMA) and their copolymers, or more inert (cage) matrices.[16–18] The most used polymer electrolyte in LOB is Poly(vinylidene fluoride) (PVDF) and its copolymer PVDF-HFP (poly(vinylidene fluoride-co-hexafluoropropylene)) because of its high solubility, good electrochemical, and mechanical features, low crystallinity and glass transition temperature, and flexibility.[19–23] In a typical procedure, PVDF-HFP is dissolved in a lithium salt solution such as $LiClO_4$, $LiPF_6$,

[a] M. Celik, Dr. S. Pakseresht, Dr. A. W. M. Al-Ogaili, S. Usta, Prof. Dr. H. Akbulut, Assoc. Prof. T. Cetinkaya
Research, Development and Application Center (SARGEM), Sakarya University, Esentepe, Sakarya 54187, Turkey
E-mail: mustafacelik@sakarya.edu.tr

[b] M. Celik, S. Usta, Prof. Dr. H. Akbulut, Assoc. Prof. T. Cetinkaya
Department of Metallurgical and Materials Engineering, Engineering Faculty, Sakarya University, Esentepe, Sakarya 54187, Turkey

[c] Prof. Dr. H. Akbulut, Assoc. Prof. T. Cetinkaya
NESSTEC Energy & Surface Technology A.S., Technology Development Zones, Sakarya University, Esentepe, Sakarya 54187, Turkey

Supporting information for this article is available on the WWW under https://doi.org/10.1002/batt.202300263

and LiTFSI in TEGDME to obtain a gel polymer electrolyte.[24,25] In our previous study, these salts were investigated in PVDF-HFP copolymer, and the best cycle stability in LOBs was determined in 1.5 M LiTFSI/TEGDME system.[26] However, relatively low ionic conductivity and low cycling properties were obtained. Therefore, the addition of ceramic filler into the polymer matrix can overcome these issues by improving ionic conductivity and cycling properties.[27,28] Ceramic fillers are classified into two groups: passive fillers that do not engage in the lithium ion conduction process (e.g., TiO_2,[29–31] SiO_2,[32–34] and Al_2O_3[35–37]) and active fillers (e.g., $Li_{0.33}La_{0.557}TiO_3$ (LLTO),[37] $Li_7La_3Zr_2O_{12}$,[38] $Li_{6.4}La_3Zr_{1.4}Ta_{0.6}O_{12}$,[39] $Li_{10}GeP_2S_{12}$,[40] and $Li_{1.7}Al_{0.3}Ti_{1.7}(PO_3)_4$ (LATP).[41] Active inorganic electrolyte fillers can improve electrochemical performance more effectively, as they not only increase the amorphous area of the polymer matrix, but also facilitate the conduction of lithium ions. Active fillers also provide extra diffusion pathways for Li^+.[42] LATP is a potential choice among active fillers because of its high ionic conductivity and good air stability. Moreover, with the addition of ceramic additives in gel polymer electrolytes, polymer amorphism and chain mobility can be increased.[21,43,44] Moreover, ceramic additives prevent the formation of impurities, which take place due to undesired reactions between the electrode and the electrolyte.[45] Therefore ceramic fillers addition is an excellent way to reduce the interfacial resistance in the lithium electrode.[30] Overcoming the electrode-electrolyte interface increases the stability of cell and minimizes the dendrite formation on the lithium metal anode. Hybrid ceramic-polymer electrolytes also can improve mechanical properties.[46–48]

Recently, double-layer polymer electrolytes have gathered the attraction of researchers. In this polymer electrolyte system, original design and polymer layer selections have been performed based on the requirements of battery chemistry and electrode materials. For example, Zhou et al.[49] reported a double-layer polymer electrolyte for LIBs. Here, while the PEO layer in the double-layer structure is designed to enable dendrite-free growth at the anode side, a poly(N-methyl-malonic amide) layer was selected on the cathode side to facilitate the extraction of Li+ ions. On the other hand, Wang et al.[50] studied a double-layer polymer electrolyte to enhance the stability of lithium-sulfur batteries. To overcome the "passivation effect" of lithium pure polyacrylonitrile (PAN) layer was located on the anode side, and to increase the ionic conductivity PEO blended and LATP dispersed polymer layer was located through the cathode side. This layer aims to mitigate the passivation effect and provide high ionic conductivity. By leveraging the inherent high ionic conductivity of PAN, this layer enhances the rate performance of the system. Regarding Li-O2 batteries, the studies have focused on the interface issues between the NASICON and Garnet type of inorganic solid electrolyte against lithium metals. To overcome the side reaction between inorganic solid electrolytes and lithium metal, the surface of inorganic solid electrolytes was coated or deposited with organic polymers such as PEGMEM.[9,39]

In this work, we present a double-layer gel polymer electrolyte for specifically Li-O_2 batteries. The developed electrolyte consists of two layers, each of which serves a particular purpose. In our previous study, we have reported that the direct coating of GPE on the cathode eliminated the contact resistance between cathode and electrolyte.[26] The first layer, referred to as GPE, involved a thin coating of PVDF-HFP dispersed with LiTFSI salt applied to the cathode. The second layer, labeled as c-GPE, incorporated LATP inorganic particles, along with integrated LiTFSI salt, layered on top of the GPE. c-GPE employed both as a protective layer to avoid Li corrosion and improve the overall ionic conductivity of the double gel polymer electrolyte (d-GPE) membranes. By employing two distinct GPE layers, one for the cathode and another serving as the electrolyte, it becomes possible to achieve a suitable energy gap and chemical durability. This compatibility enables the integration of the double-layer polymer system with both the cathode and the Li metal anode. As a result, the Li-O_2 cells constructed with such d-GPE offer an improved electrochemical characteristic.

Results and Discussion

Figure 1 depicts a schematic synthesis process of d-GPEs, which consists of three main steps. First, GPE was prepared by dissolving PVDF-HFP/acetone solution and liquid electrolyte. In the second stage, LATP ceramic particles with a range size of 0.5–5 μm were synthesized and added into GPE mixture to obtain c-GPE. At last, the GPE mixture was casted onto the GDL host cathode, and the GPE was observed to be semi-transparent and viscous. The c-GPE was then coated on the first layer, and a highly flexible double-layered GPE was formed. The replacement of liquid electrolytes with GPE in LOB has proven to be a viable solution for addressing some of the issues associated with liquid electrolytes. It could assist in protecting the Li anode from impurities in the atmospheric air while avoiding the leakage and volatilization of the liquid solvent in an open system. Moreover, to optimize the amount of LATP for c-GPE preparation, different wt.% was applied (e.g., 2.5%, 5%, and 10%). In the following section, the crystalline structure, morphology, and electrochemical performance of GPE and c-GPE with different wt% are presented. The contents and properties of the polymer electrolyte samples were listed in Table 1.

Table 1. Contents of polymer electrolyte samples and their properties.

Sample	PVDF:HFP [wt.%]	LiTFSI [mole]	LATP [wt.%]	Thickness [μm]
GPE	100	1.5	–	550
c-GPE-1	97.5	1.5	2.5	550
c-GPE-2	95	1.5	5	550
c-GPE-3	90	1.5	10	550

Research Article
doi.org/10.1002/batt.202300263
Chemistry Europe
European Chemical Societies Publishing

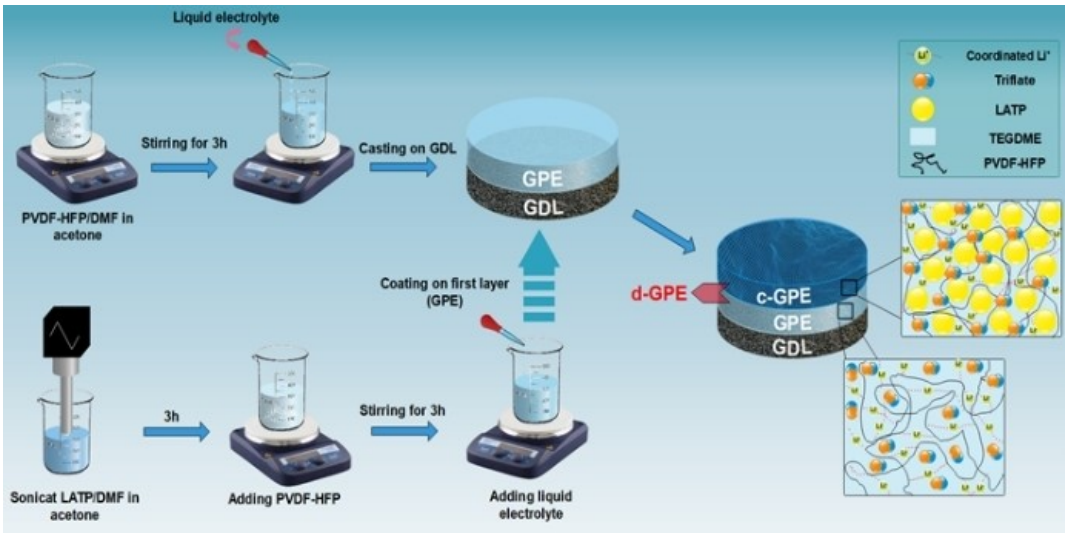

Figure 1. Schematic process of d-GPE production for lithium-oxygen battery systems.

Characterization of GPE and c-GPE

The XRD patterns of pure PVDF-HFP, GPE, and c-GPE with 2.5 wt.%, 5 wt.%, and 10 wt.% LATP (referred as c-GPE-1, c-GPE-2, and c-GPE-3, respectively) are demonstrated in Figure 2a. The semicrystalline nature of PVDF-HFP is confirmed owing to the presence of characteristic peaks at $2\theta =$ 18.2°, 20°, 26.7°, and 38° correlating to α-phase.[54,55] The peaks at 26.7° and 38° vanished after the addition of LiTFSI, and the other peaks broadened, indicating a lower degree of crystallinity in the GPE, which supports the higher ionic conductivity of the GPE system.[56,57] The improvement of conductivity can be ascribed to the accessibility of more space for ionic transport. The XRD pattern of LATP identified the positions of the sharp peaks, which are in well agreement with previous findings.[58,59] The c-GPEs revealed new peaks at $2\theta =$ 24.8°, 30.1°, 33.2°, and 37° after introducing LATP particles. These peaks became sharper with increasing wt% of LATP from 2.5% to 10%, demonstrating enhancing crystallinity of c-GPE.

For determining crystalline changes and confirming structure, FTIR spectrum analyses are valuable. Figure 2(b) displays the FTIR spectra of pure PVDF-HFP, which peaks located at

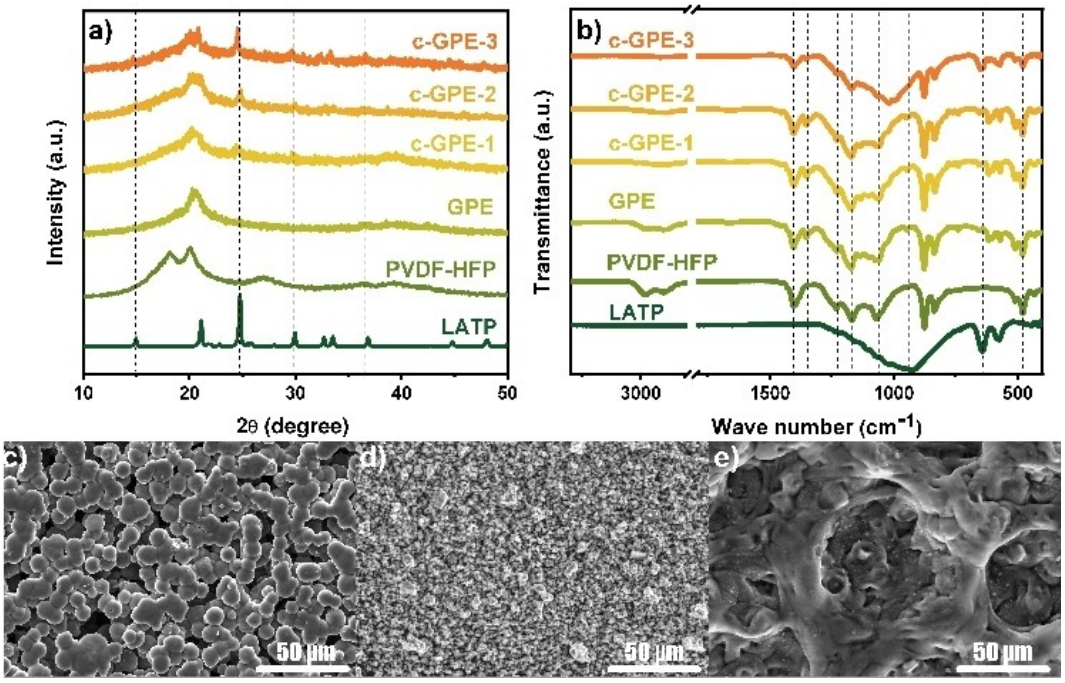

Figure 2. The a) XRD and b) FTIR spectra of PDVF-HFP, GPE, c-GPEs samples. The morphology studies of c) GPE, d) LATP, and e) c-GPE-2 by FESEM analysis.

Research Article
doi.org/10.1002/batt.202300263
Chemistry Europe
European Chemical Societies Publishing

853 cm^{-1} and 870 cm^{-1} and peaks in the range of 2000–3000 cm^{-1} attributed to α-phase of PVDF-HFP, suggesting the amorphous structure of polymer.[60] The peaks at 1100 cm^{-1}, 1200 cm^{-1}, and 1240 cm^{-1} are ascribed to C–F stretching modes of PVDF-HFP, which allows for segmental motion inside the polymer and improves ionic conductivity. The peak at 1400 cm^{-1} shows the C–H_2 scissoring vibration.[61] In FTIR pattern of GPE, the peaks in the 1140–1500 cm^{-1} region are due to dissolving LiTFSI in the gel structure. The C–H vibration modes, evident at 1422–1445 cm^{-1}, imply lithium compound accumulation in the polymer membrane. The appearing peaks at 600 cm^{-1} are owing to SO_2 groups of LiTFSI. In c-GPE samples, characteristic peaks at 580 cm^{-1}, 648 cm^{-1}, and 1041 cm^{-1} are assigned to LATP. These peaks were much visible when the wt% of LATP increased to 10%, and the organic bounds of LiTFSI were reduced.

FESEM micrographs of the surface of the as-prepared GPE and c-GPE with 5 wt.% LATP are shown in Figure 2(c and d). The GPE surface is homogenous and reveals that pores exist in the GPE (Figures 2c and S1a, b), but the porosity decreases when mixed with 5% LATP to produce a c-GPE-2 (Figures 2e and S2c, d). The as-prepared LATP particles show cubic and irregular shapes, as indicated in Figures 2(d) and S1(c, d), and uniformly were embedded in the polymer matrix, as can be seen in Figure 2(e). It is worth mentioning that increasing wt.% of LATP to 10% decreased the porosity and free volume of the GPE (Figure S2e and f). The excessive LATP loading resulted in aggregation and hence obstruction of Li^+ conducting and air-breathing channels and can be resulted in a short life cycle. The presence of an optimum loading is supported by this trade-off in the impact of adding LATP. In this study, the optimum loading quantity was found to be 5%.

The EIS technique was used to estimate the ionic conductivity of GPE, c-GPEs at room temperature, with the findings given in Figure 3(a). The ionic conductivity was determined using Equation (1), where *d*, *R*, and SA stand for GPE thickness, Nyquist pilot (bulk resistance), and surface area, respectively.

$$\sigma = \left(\frac{1}{R}\right)\frac{d}{SA} \quad (1)$$

The variation of bulk resistance and ion conductivity values for GPE, c-GPE-1, c-GPE-2, c-GPE-3 are summarized in Table S1. The c-GPEs indicate a higher ionic conductivity compared to GPE system. On the other hand, for c-GPE systems, ionic conductivity increased steadily from 3.34×10^{-5} S cm^{-1} for 2.5 wt.% LATP to a maximum value of 1.222×10^{-4} S cm^{-1} with 5 wt.% LATP. However, when the LATP filler was added, ionic conductivity improved with the addition in filler content until it reached 5%, then began to decline as the filler amount was increased to 10%. This increase can be assigned to the interaction between the LATP and the ions in the c-GPE, mainly the binding of the TFSI ions on the LATP surface and the forming of ion-LATP clusters. The ion pair dissociation is accelerated because of this interaction. This dissociation enhances the number of free Li ions, making it easier to move them along the ceramic fillers. This suggests that the development of a continuous filler network is required to improve Li^+ transport. Therefore, an optimum ceramic filler loading is necessary for improving Li ions movement.[21,62]

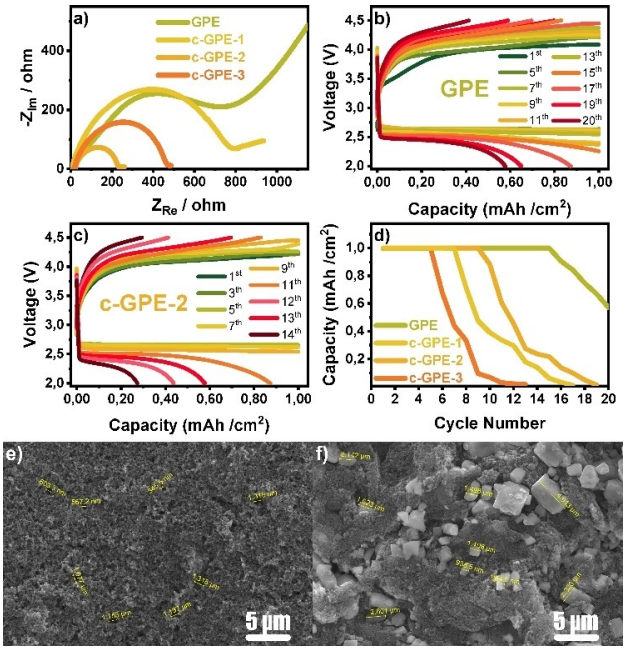

Figure 3. a) The EIS spectra of GPE and c-GPEs samples. Discharge-charge profiles of b) GPE and c) c-GPE-2 for 20 and 14 cycles at a controlled capacity of 2.5 mAh, respectively. d) Cycling performance of Li-O_2 cells with GPE and c-GPEs systems. FESEM images of GDL surface e) before and f) after coating with c-GPE-2.

The Li-O_2 cells assembled with GPE and c-GPEs systems were discharged and charged at a controlled capacity of 2.5 mAh to evaluate their cycling performances. Figure 3(b and c) indicates the voltage curves of the cells with GPE and c-GPE-2, respectively. But even though the voltage curves of the cells were initially steady, after cycling the overpotential increased, and the cell failed after 16 and 10 cycles for GPE and c-GPE-2. The shorter life cycle of c-GPE-2 can be assigned to blocking the GDL porous framework by LATP particles. Due to the preparation techniques, c-GPE was coated on the GDL and dried on it. Therefore, the nano-ceramic LATP particles penetrate through the porous of GDL and decrease the surface area where reversible Li_2O_2 reaction take place. To approve this point, the morphology surface of pristine GDL and coated GDL with c-GPE-2 were evaluated by FESEM. Figure 3(e) presents the porous structure of GDL with the width pores of 0.5–2 µm. After coating the GDL with c-GPE-2, the semitransparent form of c-GPE-2 was peeled off from GDL surface, and FESEM analysis revealed that LATP clogged the GDL pores (Figure 3f). Therefore, the blockage of GDL porous channels prevents air-breathing cathode, which leads to irreversible charge/discharge processes and, consequently, decades the cell performance. The cycling performance of the cells with c-GPE-1 and c-GPE-3 displayed stability up to 8 and 5 cycles (Figures 3d and S3). It is concluded that the amount of LATP in c-GPE plays a critical key in battery performance. Increasing the LATP up to 10 wt.% the ionic conductivity is reduced and also due to porous clogging

Research Article
doi.org/10.1002/batt.202300263
Chemistry Europe
European Chemical Societies Publishing

of the cathode surface cell is failed in early cycles. According to the results, c-GPE-2 containing 5% LATP showed the best performance and was selected for the further preparation of d-GPE. Moreover, Li symmetric cells were assembled to confirm the stability of lithium metal against c-GPE-2. As shown in Figure S6, the Li/c-GPE-2/Li cell indicated 400 hours of cycle stability at 1.0 mA cm^{-2} current density, proving compatibility with the lithium anode.

Characterization of d-GPEs

Mechanical property is a significant physical characteristic of polymer electrolytes. The stress-strain patterns of the GPE, c-GPE-2, and d-GPE at room temperature are shown in Figure 4(a). The GPE has a tensile strength of 2.6 MPa and an elongation break of 80%, whereas the c-GPE-2 and d-GPE have tensile strengths of 5.9 MPa and 3.9 MPa, respectively, with breaking tensile strengths of 110% and 100%. The stress-strain test imparted the LATP fillers could enhance the toughness of GPE by maximizing the interaction between LATP and polymer matrix. As a result, the strength of d-GPE improved, which can minimize the possibility of torsional distortion, which is advantageous for battery applications.

Furthermore, because the Li-O_2 cells run in a semi-open environment, it is critical to hamper electrolyte loss while cells are working. The evaporation of volatile compounds in the polymer electrolytes was explored using TGA under isothermal circumstances at 120 °C. The thermal behavior of GPE, c-GPE-2, and d-GPE was studied for comparison. The GPE demonstrated a weight loss of 9 wt.% of its initial mass after 2 hours, as indicated in Figure 4(b). On the other hand, the c-GPE-2 showed excellent thermal stability, and d-GPE exhibited a slight wt.% loss, suggesting the integration of c-GPE and GPE have improved the overall thermal stability of polymer electrolyte.

A flammability experiment was conducted to investigate the safety of GPE, GPE-2, and d-GPE, as seen in Figure 4(c–k). The GPE film begins to burn and shrink instantly after being ignited and continues to burn for at least 10 seconds (Figure 4c–e). In contrast, c-GPE-2 (Figure 4f–h) and d-GPE (Figure 4i–k) do not keep fire after ignition, with only a little charred area visible on the film surface and the films preserved after 10 seconds of combustion, which exhibited the efficient enhancement of safety. Therefore, the d-GPE can be used in safety-reinforced lithium batteries that run at high temperatures due to its higher thermal durability and non-flammability.[63]

To understand the contribution of GPE and c-GPE-2 in improving ionic conductivity and crystalline structure of d-GPE, the thickness of each GPE and c-GPE-2 layer was adjusted between 200–350 μm to make a total thickness of 550 μm for d-GPEs. The thickness of c-GPE-2/GPE was controlled to be 350–200 μm, 300–250 μm, 250–300 μm, and 200–350 μm, which named as d-GPE-1, d-GPE-2, d-GPE-3, d-GPE-4, respectively. The XRD result exhibited that increasing the c-GPE-2 thickness enhanced the crystallinity of d-GPE. FESEM analysis further shows d-GPE is compact from a cross-sectional aspect, with a thickness of roughly 550 μm (Figure 5b, c). The GPE is well integrated with the cathode surface and c-GPE-2.

Ionic conductivities of d-GPEs with different thicknesses of GPE and c-GPE-2 layers were evaluated and listed in Table 2.

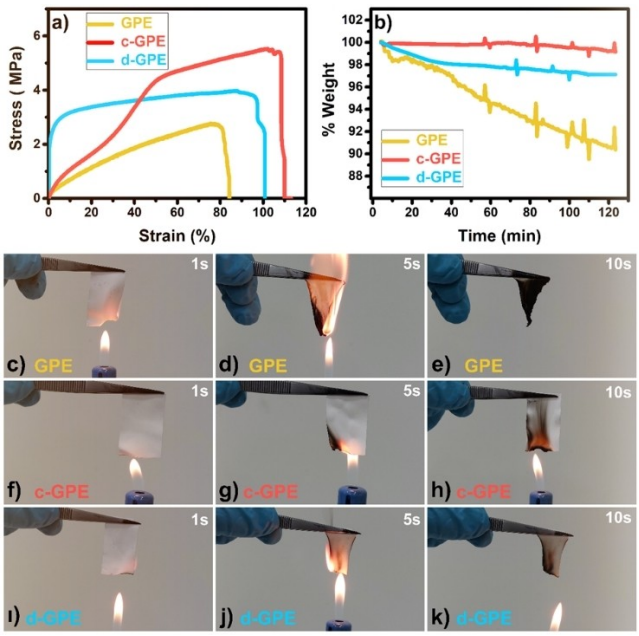

Figure 4. a) The stress-strain patterns and b) TGA profiles for GPE, c-GPE-2, and d-GPE at isothermal circumstances of 120 °C for 120 minutes. Digital images of flammability test for GPE (c–e), c-GPE-2 (f–h), and d-GPE (i–k).

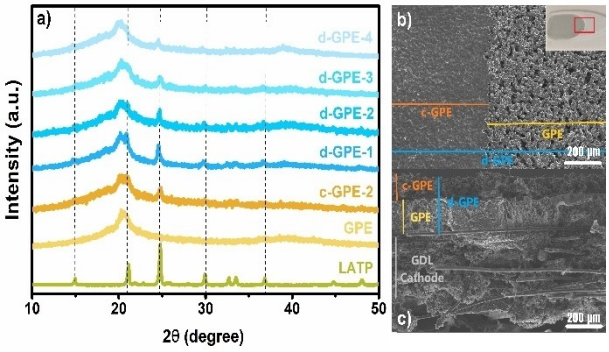

Figure 5. a) The XRD pattern of GPE, c-GPE-2, and d-GPEs samples. The cross-section view of d-GPE by FESEM in b) low and c) high magnitude.

Table 2. Bulk resistance, ionic conductivity, and Li^+ transference of GPE, c-GPE, and d-GPEs.

Polymer gel electrolyte systems	Bulk resistance	Ionic conductivity value [S cm^{-1}]	Li^+ transference number	Cycle numbers
GPE	849	3.22×10−5	0.6510	16
c-GPE-2	226	1.21×10−4	0.7353	10
d-GPE-1	382	7.16×10−5	0.7226	27
d-GPE-2	421	6.49×10−5	0.7202	34
d-GPE-3	467	5.85×10−5	0.7147	29
d-GPE-4	712	3.84×10−5	0.7061	23

Research Article
doi.org/10.1002/batt.202300263
Chemistry Europe
European Chemical Societies Publishing

From EIS spectra in Figure 6(a) can find the highest conductivity was for d-GPE-1 and d-GPE-2 when the thickness of c-GPE-2 was 350 μm and 300 μm, respectively. It is suggested that c-GPE is associated with the improvement of ionic conductivity in d-GPE system. Besides, the d-GPE has been shown to enhance Li+ ion transport characteristics and increase interfacial durability towards the Li electrode. Based on the findings of chronopotentiometry stability and impedance (Figure S4), we calculated the transference number in GPE, c-GPE-2, and d-GPEs with different thicknesses of each layer. As given in Table S2, t^+ values enhanced for d-GPEs with an increase of c-GPE thickness.

The linear sweep voltammogram was also used to understand more about the electrochemical durability of d-GPEs, and the corresponding linear sweep voltammograms are presented in Figure 6(b). According to the data, the electrochemical window of the GPE, c-GPE-2, d-GPE-1, d-GPE-2, d-GPE-3, and d-GPE-4 is 4.5 V, 5.14 V, 4.92 V, 4.87 V, 4.68 V, and 4.63, respectively. The LSV curve of samples shows no visible decomposition before 4.5 V, indicating anodic stabilities, but the GPE, d-GPE-3, and d-GPE-4 start to decompose at 5.0 V, approving the improved electrochemical durability of c-GPE, d-GPE-1, and d-GPE-2. This means c-GPE contributes to enhancing the stability of electrochemical energy storage.

The Li-O2 cells constructed with GPE, c-GPE-2, and d-GPEs were cycled at a current density of 0.25 mA at room temperature within a fixed specific capacity of 2.5 mAh. The discharge-charge curves of the cells with d-GPE-2 are shown in Figure 6(c). But even though the voltage profiles of the d-GPE-2 cell were initially steady, the overpotential increased with cycling, and the cell failed after 34 cycles. The cells with d-GPE-1, d-GPE-3, and c-GPE-4 exhibited a lifespan of 27, 29, and 23 cycles, respectively. This result could be assigned to the formation of lithium dendrites on the Li metal anode, as well as the deposition of discharge products on the cathode. The cell with GPE demonstrated substantially higher cell polarization owing to the high internal resistance within the cell. The cell with d-GPE-2 showed the best performance, demonstrating that using both GPE and c-GPE with optimized thickness and LATP content can improve the cycling stability of LOB systems.

To provide more insights on the contribution of d-GPEs on LOBs capacity, full discharge test was carried out at a current density of 0.25 mA. Figure 7(a) illustrates that cells utilizing d-GPE-2 have a maximum discharge capacity of 20.3 mAh, compared to GPE, c-GPE, d-GPE-1, d-GPE-3, and c-GPE-4, which have capacities of 7.61, 6.9, 6.6, 11.4, and 8.4 mAh, respectively. The d-GPE-2 showed the best performance, similar to the ionic conductivity and transference number tests, suggesting the impact of the enhancement of ionic conductivity and transference number of d-GPE-2 on the Li-O_2 cell. From Figure 7(b), XRD analysis detected the diffraction peaks at 32.3°, 35°, 40°, and 48.6° (JCPDS no. 09–0355), which corresponded to the formation of Li_2O_2 as the main discharge product with either polymer electrolyte. The other peak at $2\theta = 33.5°$ is correlated to LiO_2 formation (JCPDS no. 77–2144). Moreover, XRD results showed the presence of Li_2CO_3 (at 2θ: 21.2°, 30.2°; JCPDS no. 22–1141) in GPE and c-GPE-2 systems after fully discharged. It can be concluded that d-GPEs avoid the formation of parasite products (such as carboxylates and LiOH) and provide highly stable Li-O_2 cells. Besides, the formation of discharge product on the cathode was investigated by FESEM after fully discharged Li-O_2 cell. All cathodes with GPE, c-GPE, and d-GPEs

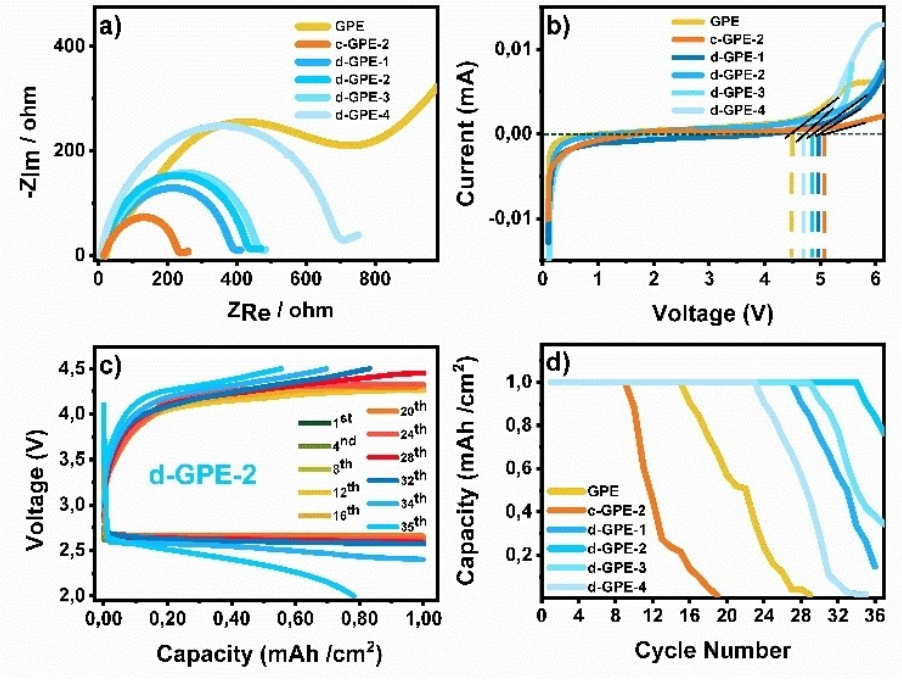

Figure 6. a) EIS and b) linear sweep voltammogram results of GPE, c-GPE-2, and d-GPEs samples. c) The voltage profiles of d-GPE-2 at a fixed capacity of 2.5 mAh. d) Cycling performance of Li-O2 cells with GPE, c-GPE-2, and d-GPEs systems.

Research Article
doi.org/10.1002/batt.202300263
Chemistry Europe
European Chemical Societies Publishing

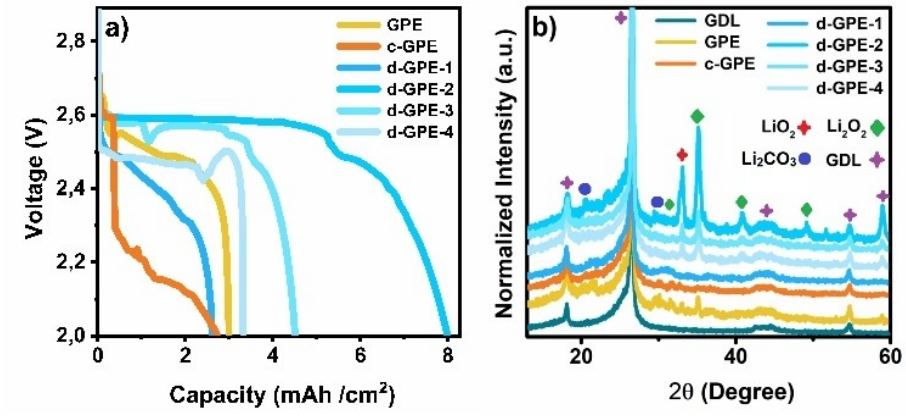

Figure 7. a) Full discharge profile of GPE, c-GPE-2, and d-GPEs at a current density of 0.25 mA. b) The XRD spectra of fully discharged cathode in GPE, c-GPE-2, and d-GPEs system.

systems revealed toroid morphology on the GDL surface after full discharge (Figure S5).

Conclusions

A double gel polymer electrolyte system was successfully applied for Li-O_2 batteries. It is found that LATP 5 wt.% ceramic additive in PVDF: HFP showed the best ionic conductivity up to 1.2104×10^{-4} S cm^{-1}, but the lowest cycle number of 10. Therefore, it was found that instead of direct application of ceramic additive polymer electrolyte on the cathode surface, a double gel polymer electrolyte system is more beneficial to enhancing the cyclability and stability of the Li-O_2 batteries. The Li-O_2 cell assembled with double gel polymer electrolyte showed an ionic conductivity of 6.49×10^{-5} S cm^{-1} and exhibited stable number of cycles up to 34 with 100% capacity retention. It is believed that such a double gel polymer electrolyte system will be an alternative method for the development of quasi-solid-state Li-O_2 batteries in the near future.

Experimental Section

Materials and synthesis method

Poly (vinylidene fluoride-co-hexafluoropropylene) (PVDF-HFP, Mw = 4105 g mol^{-1}, Aldrich), N, N- dimethylformamide (DMF, 99.9%, Aldrich), acetone (99.9%, Alpha Aesar), lithium bis (trifluoromethane sulfonyl) imide (LiTFSI) salt, tetraethylene glycol dimethyl ether (TEGMDE, ≥99%, Sigma Aldrich), titanium isopropoxide ($Ti(OCH(CH_3)_2)_4$, 99.9%, Aldrich), aluminum isopropoxide ($Al[OCH(CH_3)_2]_3$, lithium acetate ($C_2H_3LiO_2$, 99.95%, Sigma Aldrich), ammonium dihydrogen phosphate ($(NH_4)H_2PO_4$, 99.9%, Sigma Aldrich), ethylene glycol (EG) and citric acid were used as purchased, except for PVDF-HFP, which was dried in a vacuum oven at 50 °C for 6 hours.

The preparation of GPE was begun by dissolving PVDF-HFP in a mixture of DMF and acetone (DMF: Acetone ratio 3:7 wt:wt). PVDF-HFP accounts for 16 wt% of the final mixture. The mixture was then magnetically stirred for 3 hours at 450 rpm to produce a highly viscous gel. Liquid electrolytes were prepared separately by dissolving LiTFSI salt in TEGDME using magnetic stirring at 600 rpm in an argon atmosphere for 12 hours. Following that, LiTFSI/TEGDME mixture and PVDF-HFP solution were mixed with a mass ratio of 7:2. Then, the mixture was magnetically stirred for 2 hours at 50 °C and GPE solution was obtained.

For the production of composite polymer electrolytes, firstly, LATP ceramic powders were produced via the sol-gel method as previously reported by our group.[51] Briefly, solution A containing $Ti(OCH(CH_3)_2)_4$ and $Al[OCH(CH_3)_2]_3$ were dissolved in citric acid (CA) solution. Solution B was prepared by mixing $C_2H_3LiO_2$ and $(NH_4)H_2PO_4$ in CA solution. Then, Solution A and B were mixed, and subsequently, EG was added and stirred at 80 °C till a gel form was obtained. The gel was kept in an oven at 150 °C overnight, then crystalized at 500 °C under argon gas. After 5 hours, the temperature was raised to 850 °C under atmospheric air to gain the desired phase.

The as-prepared LATP were dispersed in DMF and acetone by ultrasonic treatment; after 3 hours, the mixture was then added into GPE and c-GPE was obtained. For comparison, the obtained GPE and c-GPE were coated on Gas Diffusion Layer (GDL, SIGRACET 24BC, SGL Carbon Inc.) with the same thickness of 550 μm. For double-layer GPE production, the coating thickness adjusted as 550 μm, where GPE has (550-x) μm and remain belongs to c-GPE (x) μm. The GPE was first casted on the GDL, and after a while, the c-GPE was coated on the first layer. To avoid shrinkage of the polymer, the as-cast film was kept at ambient temperature for 24 hours before being dried at 50 °C for 12 hours in the vacuum oven to extract the acetone slowly. The GPE sheets were then cut to the desired diameter (ø 18 mm) for the Li-O_2 battery application.

Characterization of gel-polymer electrolytes

A Quanta FEG 450 field emission scanning electron microscope (FESEM) was used to examine the morphology of GPEs. CuKα radiation was performed to describe X-ray diffraction (XRD) patterns on a Rigaku D/MAX 2000 X-ray diffractometer from 10° to 80° at 2θ.

To describe the impregnation of lithium salts and ceramic fillers into polymer matrices, FTIR analysis was performed in Attenuated Total Reflection (ATR) mode with 4 cm^{-1} resolutions between 400 and 4000 cm^{-1}. Universal testing devices (UTM, Instron Instruments) were used to assess the mechanical properties of the gel polymer films. The rate of extension was retained constant at 5 mm min^{-1}. The films have dimensions of 2 cm×5 cm×550 μm (width×length×-

thickness). Thermogravimetric analysis (TGA) was performed (NETZSCH STA 449 F1) to examine the volatilities of different gel polymer electrolytes using a simultaneous TGA-DTA analysis. The weight loss of the electrolytes was monitored under isothermal conditions (120 °C) under nitrogen gas flow for 2 h. Flame tests was carried out by direct observation of electrolyte ignition and combustion.

Cell-assembly and electrochemical analysis

Test cells (EL-Cell, ECC-Air) were assembled in a glovebox to evaluate the electrochemical performance of GPEs, with lithium, GPE, and GDL serving as an anode, electrolyte, and cathode, respectively. The ionic conductivity was measured using electrochemical impedance spectroscopy (EIS) at 10 mV AC between 0.1 Hz and 1.0 MHz in symmetric Li/GPE/Li cells. Using the DC polarization approach, the lithium-ion transference number (t_{Li^+}) was estimated for GPEs in symmetric Li/GPE/Li cells.[52] Before and after polarization, EIS measurements were recorded, and the lithium ion transference number was determined using the Bruce-Vincent-Evans equation (as seen below).[53]

$$t_{Li^+} = \frac{I_s(V - I_0R_0)}{I_0(V - I_sR_s)} \quad (2)$$

R_0 and R_s are interfacial resistances determined before and after polarization by EIS measurement, while I_0 and I_s are initial and steady state currents on the DC polarization curve. 0.01 V was used as the polarization voltage. In a Li/GPE/SS (stainless steel) cell, linear sweep voltammetry (LSV) was applied to determine the electrochemical window of GPEs between 0 and 6 V using a 0.1 $mV\,s^{-1}$ scanning rate. The anodic and cathodic processes, as well as their related voltages, were observed in a Li/GPE/GDL cell using cyclic voltammetry with a scan rate of 0.2 $mV\,s^{-1}$. In a Li/GPE/GDL cell with a current density of 0.1 $mA\,cm^{-2}$, 10 h time-limited galvanostatic charge-discharge tests were performed between 2.0 and 4.5 V. All electrochemical measurements were carried out at room temperature using a Gamry Ref. 1000 potentiostat-galvanostat equipment.

Acknowledgements

The authors thank the TUBITAK for supporting this work under contract number 217M979 and the European Interest Group EIG CONCERT-Japan. Sakarya University Scientific Research Projects Coordination Unit under grant number 2021-18-42-96 and 2021-18-42-95.

Conflict of Interests

The authors declare no conflict of interest.

Data Availability Statement

The data that support the findings of this study are available from the corresponding author upon reasonable request.

Keywords: gel polymer electrolyte · battery cyclability · electrochemical performance · quasi-solid-state · lithium-O_2 batteries

[1] L. Leng, X. Zeng, P. Chen, T. Shu, H. Song, Z. Fu, H. Wang, S. Liao, *Electrochim. Acta* **2015**, *176*, 1108–1115.
[2] H. G. Jung, J. Hassoun, J. B. Park, Y. K. Sun, B. Scrosati, *Nat. Chem.* **2012**, *4*, 579–585, DOI 10.1038/nchem.1376.
[3] K. Zhang, S. Mu, W. Liu, D. Zhu, Z. Ding, Y. Chen, *Ionics* **2019**, *25*, 25–33, DOI 10.1007/s11581-018-2580-9.
[4] W. Xu, V. V. Viswanathan, D. Wang, S. A. Towne, J. Xiao, Z. Nie, D. Hu, J. G. Zhang, *J. Power Sources* **2011**, *196*, 3894–3899, DOI 10.1016/j.jpowsour.2010.12.065.
[5] R. Padbury, X. Zhang, *J. Power Sources* **2011**, *196*, 4436–4444 DOI 10.1016/j.jpowsour.2011.01.032.
[6] M. Balaish, A. Kraytsberg, Y. Ein-Eli, *Phys. Chem. Chem. Phys.* **2014**, *16*, 2801–2822, DOI 10.1039/c3cp54165g.
[7] M. Salado, E. Lizundia, *Mater. Today Energy* **2022**, *28*, 101064.
[8] S. Lee, S. Jung, S. Yang, J. H. Lee, H. Shin, J. Kim, S. Park, *Appl. Surf. Sci.* **2022**, *586*, 152790, DOI 10.1016/j.apsusc.2022.152790.
[9] Z. Gu, X. Xin, J. Yang, D. Guo, S. Yang, J. Wu, Y. Sun, X. Yao, *ACS Appl. Energ. Mater.* **2022**, *5*, 9149–9157.
[10] S. Bonizzoni, C. Ferrara, V. Berbenni, U. Anselmi-Tamburini, P. Mustarelli, C. Tealdi, *Phys. Chem. Chem. Phys.* **2019**, *21*, 6142–6149, DOI 10.1039/c9cp00405j.
[11] E. jeong Yi, K. young Yoon, H. A. Jung, T. Nakayama, M. jung Ji, H. Hwang, *Appl. Surf. Sci.* **2019**, *473*, 622–626, DOI 10.1016/j.apsusc.2018.12.202.
[12] A. Manthiram, X. Yu, S. Wang, *Nat. Rev. Mater.* **2017**, *2*, 16103.
[13] J. M. Tarascon, M. Armand, *Nature* **2001**, *414*, 359–67.
[14] A. K. Tripathi, *Mater. Today Energy* **2021**, *20*, 100643.
[15] S. H. Siyal, M. Li, H. Li, J.-L. Lan, Y. Yu, X. Yang, *Appl. Surf. Sci.* **2019**, *494*, 1119–1126.
[16] S. Li, S. Q. Zhang, L. Shen, Q. Liu, J. Bin Ma, W. Lv, Y. B. He, Q. H. Yang, *Adv. Sci.* **2020**, *7*, 1903088, DOI 10.1002/advs.201903088.
[17] W. Li, Y. Wu, J. Wang, D. Huang, L. Chen, G. Yang, *Eur. Polym. J.* **2015**, *67*, 365–372, DOI 10.1016/j.eurpolymj.2015.04.014.
[18] X. Liu, X. Xin, L. Shen, Z. Gu, J. Wu, X. Yao, *ACS Appl. Energ. Mater.* **2021**, *1 (6)*, 2664–2670, DOI 10.1021/acsaem.1c00344.
[19] Shalu, V. K. Singh, R. K. Singh, *J. Mater. Chem. C* **2015**, *3* 7305–7318, DOI 10.1039/c5tc00940e.
[20] X. Tang, R. Muchakayala, S. Song, Z. Zhang, A. R. Polu, *J. Ind. Eng. Chem.* **2016**, *37*, 67–74, DOI 10.1016/j.jiec.2016.03.001.
[21] Q. Sun, X. Chen, J. Xie, C. Shen, Y. Jin, C. Huang, X. Xu, J. Tu, B. Wang, T. Zhu, X. Zhao, J. Cheng, *Mater. Today Energy* **2021**, *21*, 100841.
[22] X. Wu, Y. Ivry, J. Zheng, P. Zhang, Z. Zheng, D. Q. Tan, *Mater. Today Energy* **2023**, *31*, 101209.
[23] Y. Xia, X. Wang, X. Xia, R. Xu, S. Zhang, J. Wu, Y. Liang, C. Gu, J. Tu, *Chemistry* **2017**, *23*, 15203–15209.
[24] T. Liu, Z. Chang, Y. Yin, K. Chen, Y. Zhang, X. Zhang, *Solid State Ionics* **2018**, *318*, 88–94.
[25] J. Zhang, B. Sun, X. Xie, K. Kretschmer, G. Wang, *Electrochim. Acta* **2015**, *183*, 56–62.
[26] M. Celik, A. Kızılaslan, M. Can, T. Cetinkaya, H. Akbulut, *Electrochim. Acta* **2021**, *371*, 137824.
[27] F. Croce, G. B. Appetecchi, L. Persi, B. Scrosati, *Nature* **1998**, *394*, 456–458, DOI 10.1038/28818.
[28] R. Prasanth, N. Shubha, H. H. Hng, M. Srinivasan, *Eur. Polym. J.* **2013**, *49*, 307–318.
[29] F. Croce, R. Curini, A. Martinelli, L. Persi, F. Ronci, B. Scrosati, R. Caminiti, *J. Phys. Chem. B* **1999**, *103 (48)*, 10632–10638, DOI 10.1021/jp992307u.
[30] J. D. Jeon, M. J. Kim, S. Y. Kwak, *J. Power Sources* **2006**, *162*, 1304–1311, DOI 10.1016/j.jpowsour.2006.08.022.
[31] P. Raghavan, J. W. Choi, J. H. Ahn, G. Cheruvally, G. S. Chauhan, H. J. Ahn, C. Nah, *J. Power Sources* **2008**, *184*, 437–443, Doi 10.1016/j.jpowsour.2008.03.027.
[32] C. Capiglia, P. Mustarelli, E. Quartarone, C. Tomasi, A. Magistris, *Solid State Ionics* **1999**, *118*, 73–79, DOI 10.1016/s0167-273800457-3.
[33] P. G. Bruce, *Solid State Ionics* **2008**, *179 (21–26)*, 752–760, DOI 10.1016/j.ssi.2008.01.095.
[34] D. Saikia, A. Kumar, *Eur. Polym. J.* **2005**, *41*, 563–568, DOI 10.1016/j.eurpolymj.2004.10.029.

[35] W. Krawiec, L. G. Scanlon, J. P. Fellner, R. A. Vaia, S. Vasudevan, E. P. Giannelis, *J. Power Sources* **1995**, *54*, 310–315, DOI 10.1016/0378-775302090-P.
[36] P. A. R. D. Jayathilaka, M. A. K. L. Dissanayake, I. Albinsson, B. E. Mellander, *Electrochim. Acta* **2002**, *47*, 3257–3268, DOI 10.1016/S0013-468600243-8.
[37] H. Li, M. Li, S. H. Siyal, M. Zhu, J. Le Lan, G. Sui, Y. Yu, W. Zhong, X. Yang, *J. Membr. Sci.* **2018**, *555*, 169–176, DOI 10.1016/j.memsci.2018.03.038.
[38] A. A. AbdelHamid, J. L. Cheong, J. Y. Ying, *Nano Energy* **2020**, *71*, 104633, DOI 10.1016/j.nanoen.2020.104633.
[39] Z. Gu, X. Xin, Z. Xu, J. He, J. Wu, Y. Sun, X. Yao, *Adv. Funct. Mater.* **2023**, *33*, 2301583, DOI 10.1002/adfm.202301583.
[40] S. Tang, W. Guo, Y. Fu, *Adv. Energy Mater.* **2021**, *11*, 2000802.
[41] Y. Huang, Z. Zhang, H. Gao, J. Huang, C. Li, *Solid State Ionics* **2020**, *356*, 115437.
[42] K. Luo, L. Yi, X. Chen, L. Yang, C. Zou, X. Tao, H. Li, T. Wu, X. Wang, *J. Electroanal. Chem.* **2021**, *895*, 115462.
[43] F. Zheng, M. Kotobuki, S. Song, M. O. Lai, L. Lu, *J. Power Sources* **2018**, *389*, 198–213.
[44] P. Utpalla, S. K. Sharma, K. Sudarshan, V. Kumar, P. K. Pujari, *Eur. Polym. J.* **2019**, *117*, 10–18.
[45] H. Mazor, D. Golodnitsky, E. Peled, W. Wieczorek, B. Scrosati, *J. Power Sources* **2008**, *178*, 736–743, DOI 10.1016/j.jpowsour.2007.09.056.
[46] T. Pareek, S. Dwivedi, S. A. Ahmad, M. Badole, S. Kumar, *J. Alloys Compd.* **2020**, *824*, 153991, DOI 10.1016/j.jallcom.2020.153991.
[47] A. Das, S. Sahu, M. Mohapatra, S. Verma, A. J. Bhattacharyya, S. Basu, *Mater. Today Energy* **2022**, *29*, 101118.
[48] D. Li, L. Cao, C. Liu, G. Cao, J. Hu, J. Chen, G. Shao, *Appl. Surf. Sci.* **2019**, *493*,1326–1333 DOI 10.1016/j.apsusc.2019.07.041.
[49] W. Zhou, Z. Wang, Y. Pu, Y. Li, S. Xin, X. Li, J. Chen, J. B. Goodenough, *Adv. Mater.* **2019**, *31*, 1805574.
[50] X. Wang, X. Hao, Y. Xia, Y. Liang, X. Xia, J. Tu, *J. Membr. Sci.* **2019**, *582*, 37–47.
[51] A. Kızılaslan, M. Kırkbınar, T. Cetinkaya, H. Akbulut, *Phys. Chem. Chem. Phys.* **2020**, *22*, 17221–17228.
[52] S. Kim, S. J. Park, *Electrochim. Acta* **2009**, *54*, 3775–3780, DOI 10.1016/j.electacta.2009.01.070.
[53] J. Evans, C. A. Vincent, P. G. Bruce, *Polymer* **1987**, *28*, 2324–2328 DOI 10.1016/0032-386190394-6.
[54] K. N. Jung, J. I. Lee, J. H. Jung, K. H. Shin, J. W. Lee, *Chem. Commun.* **2014**, *50*, 5458–5461, DOI 10.1039/c4cc01243g.
[55] A. M. Stephan, K. S. Nahm, M. Anbu Kulandainathan, G. Ravi, J. Wilson, *Eur. Polym. J.* **2006**, *42*, 1728–1734.
[56] B. Luo, W. Wang, Q. Wang, W. Ji, G. Yu, Z. Liu, Z. Zhao, X. Wang, S. Wang, J. Zhang, *Chem. Eng. J.* **2023**, *460*,141329, DOI 10.1016/j.cej.2023.141329.
[57] S. Song, X. Qin, Y. Ruan, W. Li, Y. Xu, D. Zhang, J. Thokchom, *J. Power Sources* **2020**, *461*, 228146, DOI 10.1016/j.jpowsour.2020.228146.
[58] X. Liu, J. Fu, C. Zhang, *Nanoscale Res. Lett.* **2016**, *11*, 551, DOI 10.1186/s11671-016-1768-z.
[59] M. D. Singh, A. Dalvi, D. M. Phase, Y. Kumar, *J. Mater. Sci.* **2020**, *55*, 3951–3963, DOI 10.1007/s10853-019-04234-9.
[60] N. Aliahmad, S. Shrestha, K. Varahramyan, M. Agarwal, *AIP Adv.* **2016**, *6*, 065206 DOI 10.1063/1.4953811.
[61] L. M. McGrath, J. Jones, E. Carey, J. F. Rohan, *ChemistryOpen* **2019**, *8*, 1429–1436, DOI 10.1002/open.201900313.
[62] A. Chamaani, N. Chawla, M. Safa, B. El-Zahab, *Electrochim. Acta* **2017**, *235*, 56–63, DOI 10.1016/j.electacta.2017.03.064.
[63] J. Gou, W. Liu, A. Tang, H. Xie, *Eur. Polym. J.* **2021**, *158*, 110703, DOI 10.1016/j.eurpolymj.2021.110703.

Manuscript received: June 22, 2023
Revised manuscript received: August 14, 2023
Accepted manuscript online: August 15, 2023
Version of record online: August 30, 2023